

X-ray crystallographic observation of “*in-line*” and “*adjacent*” conformations in a bulged self-cleaving RNA/DNA hybrid

VALENTINA TERESHKO,¹ SCOT T. WALLACE,² NASSIM USMAN,³
FRANCINE E. WINCOTT,³ and MARTIN EGLI¹

¹Department of Biological Sciences, Vanderbilt University, Nashville, Tennessee 37235, USA

²Department of Molecular Biology, Intercell G.m.b.H., A-1030 Vienna, Austria

³Department of Chemistry and Biochemistry, Ribozyme Pharmaceuticals Inc., Boulder, Colorado 80301, USA

ABSTRACT

The RNA strand in an RNA/DNA duplex with unpaired ribonucleotides can undergo self-cleavage at bulge sites in the presence of a variety of divalent metal ions (Hüsken et al., *Biochemistry*, 1996, 35:16591–16600). Transesterification proceeds via an *in-line* mechanism, with the 2'-OH of the bulged nucleotide attacking the 3'-adjacent phosphate group. The site-specificity of the reaction is most likely a consequence of the greater local conformational freedom of the RNA backbone in the bulge region. A standard A-form backbone geometry prohibits formation of an *in-line* arrangement between 2'-oxygen and phosphate. However, the backbone in the region of an unpaired nucleotide appears to be conducive to an *in-line* approach. Therefore, the bulge-mediated phosphoryl transfer reaction represents one of the simplest RNA self-cleavage systems. Here we focus on the conformational features of the RNA that underlie site-specific cleavage. The structures of an RNA/DNA duplex with single ribo-adenosyl bulges were analyzed in two crystal forms, permitting observation of 10 individual conformations of the RNA bulge moiety. The bulge geometries cover a range of relative arrangements between the 2'-oxygen of the bulged nucleotide and the P-O5' bond (including *adjacent* and near *in-line*) and give a detailed picture of the conformational changes necessary to line up the 2'-OH nucleophile and scissile bond. Although metal ions are of crucial importance in the catalysis of analogous cleavage reactions by ribozymes, it is clear that local strain or conformational flexibility in the RNA also affect cleavage selectivity and rate (Soukup & Breaker, *RNA*, 1999, 5:1308–1325). The geometries of the RNA bulges frozen out in the crystals provide snapshots along the reaction pathway prior to the transition state of the phosphoryl transfer reaction.

Keywords: DNA; hydrogen bonding; nucleotide bulge; phosphoryl transfer; ribozyme; RNA; X-ray crystallography

INTRODUCTION

Following the discovery of the catalytic properties of RNA some 20 years ago (Kruger et al., 1982; Guerrier-Takada et al., 1983), many more self-splicing introns belonging to two distinct groups along with three types of small self-cleaving ribozymes have been identified. These are the hammerhead (Hutchins et al., 1986; Prody et al., 1986; Uhlenbeck, 1987; Verma et al., 1997), the hairpin (Buzayan et al., 1986; Hampel & Tritz, 1989; Hampel, 1998; Walter & Burke, 1998), and the delta ribozymes (Sharmeen et al., 1988; Wu et al., 1989). Two types of reactions are mediated by these ribo-

zymes, namely RNA splicing and site-specific RNA cleavage (Cech, 1987). In the case of the three above classes of self-cleaving ribozymes, the autolytic processing reaction proceeds with inversion of configuration of the phosphate group, as initially established with hammerhead-type ribozymes (van Tol et al., 1990; Koizumi & Ohtsuka, 1991; Slim & Gait, 1991).

A general feature of ribozymes is that they either require or are at least stimulated by divalent metal cations (Dahm & Uhlenbeck, 1991; Dahm et al., 1993). Many of the natural ribozymes show rather broad metal-ion specificity. Thus, hammerhead-type ribozymes are active with several earth alkali cations (Mg²⁺, Ca²⁺, Sr²⁺) or transition metal cations (Mn²⁺, Co²⁺, Zn²⁺) (Dahm & Uhlenbeck, 1991). Detailed analysis of the metal-ion dependence of cleavage reactions mediated by ribozymes provides evidence that the precise role of

Reprint requests to: Martin Egli, Department of Biological Sciences, Vanderbilt University, Nashville, Tennessee 37235, USA; e-mail: martin.egli@vanderbilt.edu.

the metal ions varies considerably between different classes of ribozymes. For example, RNA catalysis in the case of the hairpin ribozyme does not involve direct coordination of magnesium to the phosphate ester, nor activation of a bound water molecule, as demonstrated by efficient pH-independent cleavage in the presence of cobalt hexammine (Hampel & Cowan, 1997; Nesbitt et al., 1997; Young et al., 1997; Fedor, 2000). In addition, it was shown that aminoglycoside antibiotics or spermine alone can promote efficient hairpin cleavage with rates similar to the magnesium-dependent reaction (Earnshaw & Gait, 1998). Similarly, the Hepatitis delta virus ribozyme does not require high concentrations of metal ions for activity, perhaps due to a particular cytosine that could act as the general base in the cleavage reaction (Ferré-D'Amaré et al., 1998; Perrotta et al., 1999; Westhof, 1999; Nakano et al., 2000). This situation differs from the one in the hammerhead ribozyme, where the specific relationship between the pK_a s of metal ions and the pH-rate profile suggests that a metal hydroxide bound to the RNA acts as the base in the cleavage mechanism (Dahm et al., 1993). In general, two classes of ion-binding sites can be differentiated, namely those that bind cations that are functionally involved in catalysis, and others that bind cations that are involved in structure-stabilizing interactions and promotion of global RNA folding (Grosshans & Cech, 1989).

Neither chemical, biochemical, biophysical, structural or computational studies (Mei et al., 1989; Uebayasi et al., 1994; Setlik et al., 1995; Uchimaru et al., 1996; Herman et al., 1997, 1998; Lyne & Karplus, 2000; Torres & Bruice, 2000), alone or in combination, have yielded a consistent picture of the precise involvement of the metal-ion cofactor in the catalytic step. A possible mechanism could consist of a single solvated Mg^{2+} -hydroxide bound to the pro- R_P oxygen of the phosphate, which abstracts a proton from the 2'-OH and delivers a proton to the 5'-oxyanion leaving group (Haydock & Allen, 1985; Kuimelis & McLaughlin, 1996). Alternatively, two metal ions could participate. The first one could mediate proton transfer from the 2'-OH, and the other could stabilize the 5'-oxyanion leaving group (Steitz & Steitz, 1993; Uebayasi et al., 1994; Sawata et al., 1995; Lott et al., 1998). The latter mechanism has been implicated in enzymes involved with phosphoester hydrolysis reactions, such as those catalyzed by alkaline phosphatase (Kim & Wyckoff, 1991), phospholipase-C (Hough et al., 1989), DNA polymerase (Beese & Steitz, 1991; Brautigam & Steitz, 1998), adenylyl cyclase (Tesmer et al., 1999), and many nucleases (Gerlt, 1993).

RNA cleavage normally occurs in unpaired, nonstem regions that are involved in tertiary interactions (Brown et al., 1985; Pley et al., 1994; Scott et al., 1995; Wedekind & McKay, 1999; Nowakowski et al., 1999). A basic requirement for efficient site-specific cleavage is sufficient flexibility of the backbone to accommodate the structural changes necessary to allow the *in-line* ar-

range of attacking ($O2'$) and leaving groups ($O5'$) during the transesterification reaction (Fig. 1; Westheimer, 1968; Usher & McHale, 1976). Specifically, transesterification was demonstrated to be proportional to the *in-line* character of the internucleotide linker (Soukup & Breaker, 1999). It was shown that induction of mismatches or single- and double-base bulges into an RNA single strand via pairing to an otherwise complementary oligonucleotide leads to site-specific RNA cleavage in the presence of Mg^{2+} and other divalent metal cations (Hüsken et al., 1996). Cleavage occurs relatively specifically on the 3' side of bulged nucleotides and the products of the cleavage reaction are analogous to the one catalyzed by the hammerhead ribozyme, namely a 2',3'-cyclic phosphate (the former bulged nucleotide) and a free 5'-hydroxyl group. The actual cleavage rate in the bulge system is considerably reduced compared with the hammerhead (at least a factor of 10). Moreover, bulge-mediated cleavage is less specific compared with the hammerhead ribozyme. This is not surprising given the structural simplicity of the bulge system. As "minimal" RNA self-cleavage motifs, bulged RNA/DNA duplexes may nevertheless prove useful for studies of the *in-line* phosphoryl transfer mechanism with structural or computational tools.

The structural features of cleavage sites in catalytic RNAs were investigated with X-ray crystallographic techniques for the lead-binding pocket in tRNA^{Phe} (Brown et al., 1985), the hammerhead ribozyme (Pley et al., 1994; Scott et al., 1995) and the leadzyme (Wedekind & McKay, 1999). The early crystallographic work on the hammerhead ribozyme involved species with chemical modifications: a 2'-*O*-methylated nucleotide at the active site to prevent cleavage (Scott et al., 1995) and a hybrid composed of a catalytic RNA and a DNA substrate (Pley et al., 1994). Neither these two structures nor a more recent one of an all-RNA intermediate species (Scott et al., 1996) display a near *in-line* arrangement of the 2'-hydroxyl group with respect to the scissile P-O5' bond. A new crystal structure of the ham-

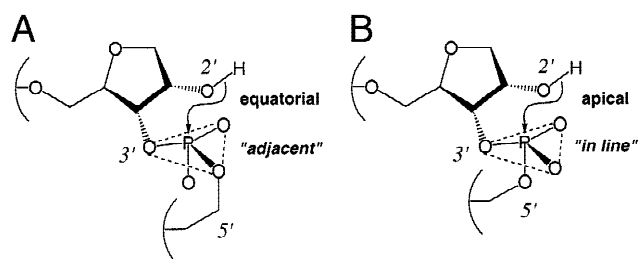


FIGURE 1. Stereochemical reaction path of phosphate ester transesterifications (Westheimer, 1968). **A:** In a canonical RNA double helix self-cleavage is prohibited due to conformational restrictions of the *equatorial* or *adjacent* relative orientation between ribose 2'-OH and adjacent phosphate group. **B:** A basic requirement for cleavage is sufficient conformational flexibility in the backbone to allow an *apical* or *in-line* orientation between 2'-OH and scissile P-O5' bond, for example, 3' adjacent to a bulged residue.

merhead with a *talo*-modification appears to display a conformation at the active site that is somewhat closer to an *in-line* arrangement (Murray et al., 1998). However, it cannot be ruled out at the moment that the conformational change is partly caused by the chemical modification and may not represent an active conformation of the native ribozyme. Although the crystal structures have yielded a detailed picture of the three-dimensional fold of the RNA, they have not helped to explain the specificity of the cleavage reaction. However, it is interesting that the captured intermediate of the cleavage-active hammerhead in the crystal showed binding of a Mg^{2+} to the pro- R_P oxygen of the attacked phosphate, consistent with the results of so-called manganese rescue experiments (Scott et al., 1996, and cited literature). In addition, the crystallographic results provide some evidence that the structural changes necessary to bring about the *in-line* conformation may occur predominantly at the local level, consistent with observations based on transient electric birefringence measurements in solution (Amiri & Hagerman, 1996). Although extensive chemical probing of the hammerhead ribozyme has yielded important insights into the role of individual residues and chemical moieties, the precise mechanism by which this structure catalyzes bond cleavage at a specific location remains a mystery (McKay, 1996).

We previously analyzed the structure of an RNA/DNA duplex with single A bulges by X-ray crystallography (Portmann et al., 1996). Cleavage in the presence of Mg^{2+} during crystallization was prevented by incorporating DNA residues at the bulge sites. To assess the relative orientation of the 2'-OH relative to the scissile P-O5' bond, the hydroxyl group was then modeled onto the deoxyribose of bulged As. In the present contribution, we report the crystal structures of the cleavage-active RNA/DNA oligonucleotide r(GCG)d(ATAT)r(ACGU) (Fig. 2), which adopts an A-form decamer duplex with two *ribo*-adenosine bulges (underlined throughout the text) in the crystal. Two crystal forms were obtained in the presence of spermine (SPM form) and spermidine (SPD form) and refined to 1.65 Å and 2.40 Å, respectively. The SPM form contains three duplexes (six A bulges) and one spermine molecule and the SPD form contains two duplexes (four A bulges) and one spermidine molecule per asymmetric unit. The numbering of residues in the individual duplexes in the SPM and SPD forms is defined in the caption of Figure 2. As in the earlier study, all bulged adenosines adopt extrahelical conformations. Together with the two 2'-deoxy A bulges previously observed in the cleavage-inactive fragment, the crystallographic data represent 12 independent observations of the same bulge moiety. Analysis of the geometries of these bulges shows that the relative orientations between bulge 2'-hydroxyl group and P-O5' bond from the 3'-adjacent C residue range from *adjacent* to near *in-line* (Fig. 1). Comparison be-

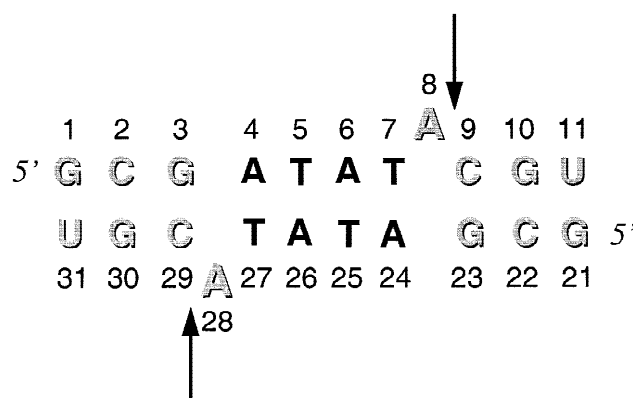


FIGURE 2. Secondary structure and numbering of the RNA/DNA duplex used in the X-ray crystallographic experiments. Ribonucleotides are gray, deoxyribonucleotides are black, and the major cleavage sites are indicated by arrows. Residues of the second duplex in the asymmetric units in the SPM and SPD forms are numbered 101–111 and 121–131 (the bulged As are residues 108 and 128). Residues of the third duplex in the SPM-form crystal are numbered 201–211 and 221–231 (the bulged As are residues 208 and 228).

tween the conformations of the r(ApC) dimers that comprise the cleavage site reveals strong correlations between several geometrical parameters, including backbone torsion angles, bulge ribose pucker, O2'(A)···P(C) distance and O2'(A)-P(C)-O5'(C) angle. Here, we describe the structural features of the bulged RNA/DNA duplexes and discuss the conformational changes that take place in the bulge-mediated RNA self-cleavage reaction during line-up of the 2'-OH and scissile phosphate bond. Although the results are discussed in the context of the phosphate transesterification reaction catalyzed by the hammerhead ribozyme, we would like to emphasize that the present conformations are not a bona-fide model for hammerhead cleavage.

RESULTS AND DISCUSSION

Cleavage experiments with a bulged RNA 11mer in solution

When exposed to Mg^{2+} in solution at ambient temperatures, the 11mer r(GCGAUUAACGC) undergoes cleavage 3' adjacent to the bulged adenosines (Fig. 3), consistent with cleavage at such sites based on solution studies with longer bulged fragments at higher temperatures (Hüsken et al., 1996). Not unexpectedly, the specificity of cleavage reactions with the shorter construct is somewhat reduced compared with the longer hybrids between 30mer oligodeoxynucleotides and longer RNA targets, featuring extended base-paired arms on either side of the bulge (Hüsken et al., 1996). Even with the latter, the specificity of bulge-mediated phosphate ester transesterification reactions is inferior to those catalyzed by the hammerhead ribozyme. However, both the hammerhead-catalyzed and the slower

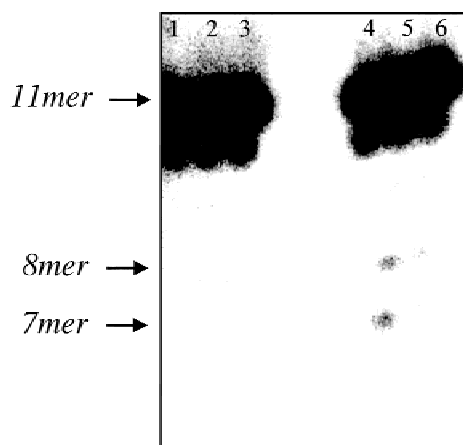


FIGURE 3. PAGE gel of cleavage reactions in solution with the RNA 11mer r(GCGAUAUACGU) (bulge underlined). Conditions were pH 6 (lanes 1–3) and pH 8 (lanes 4–6) and either in the absence of Mg^{2+} (lanes 1 and 4), or supplemented by 1 mM Mg^{2+} (lanes 2 and 5) or 5 mM Mg^{2+} (lanes 3 and 6). When judging the specificity of the bulge-mediated cleavage reactions, it is important to keep in mind that the lengths of double-stranded regions around the bulge in the 11mer construct are very short, not comparable to the longer arms used for hybridization in the original gel cleavage assays (Hüsken et al., 1996), or to typical hammerhead constructs studied both in solution and the solid state. The 10mer band visible in the gel is thought to arise from clipping of the 3'-terminal U. Nevertheless, apart from the 10mer, the bulge-mediated cleavage product, the octamer 5'-r(GCGAUAUA), represents a major band.

and less specific bulge-mediated cleavage reaction can proceed with catalytic turnover.

We would like to point out that the fact that our crystallographic construct contains DNA residues has no bearing on the study of the actual RNA cleavage site. The choice of this particular fragment is rather a consequence of its favorable crystallization properties and the resulting relatively high resolution of the diffraction data. Similarly, the hammerhead ribozyme tolerates extensive DNA substitution in its arms and specific core areas without a significant reduction of cleavage specificity and efficiency (Dahm & Uhlenbeck, 1990; Perreault et al., 1990). Indeed, a recently described RNA-cleaving DNA enzyme was shown to operate with superior catalytic efficiency (k_{cat}/K_m) compared with the hammerhead ribozyme (Santoro & Joyce, 1997).

Duplex packing in the spermine- and spermidine-form crystals

The resolution of the X-ray diffraction data collected for the two crystal forms of the RNA/DNA fragment r(GCG)d(ATAT)r(ACGU) allows visualization of all bulged residues. Electron density maps around specific regions in both crystal forms are depicted in Figure 4. The space group for the SPM and SPD forms is orthorhombic $P2_12_12_1$ (Table 1) and the asymmetric unit of the former is made up of three duplexes whereas the latter contains two duplexes. In both cases, the

duplexes form endless stacks running along the crystallographic c -axis. In the SPM form, duplexes within three-helix units are stacked with twists of -34° and -35° between terminal base pairs. At the interface between adjacent three-helix units, the helical twist is positive (23°). By comparison, in the SPD form, the helical twists are negative, both at the transition between duplexes constituting the asymmetric unit (-39°) and between adjacent two-helix units (-36°).

Growth of a particular crystal form of the 11mer is related to the nature of the polyamine used in the crystallization buffer. Variation of the pH between 5.0 and 9.0 always yielded SPM and SPD form crystals from solutions supplemented with spermine and spermidine, respectively. Analysis of the structures revealed a single polyamine molecule per asymmetric unit in both crystals. The spermine molecule is located near the stacking interface of duplexes, whereas the spermidine molecule is found between two neighboring stacks. Despite similar packing densities, SPM-form crystals diffract to higher resolution than SPD-form crystals (Table 1; data collections at the APS synchrotron with crystals of the latter form did not lead to an improvement in resolution; note the higher mosaicity of SPD-form crystals). This disparity is associated with specific lateral interactions between duplexes found in the SPM form, mediated by 2'-hydroxyl groups. In the SPM-form crystal, the interface with positive twist between two adjacent duplexes in one stack and the one with negative twist between two duplexes within a three-helix unit from another display a relative shift of approximately 1 bp along the crystallographic c -axis (Fig. 5A). At this site, a ribose zipper (Cate et al., 1996) stitches together all four duplexes, with 2'-hydroxyl groups from six different backbones forming hydrogen bonds to adjacent 2'-hydroxyls, phosphate oxygens, or base functions (O2 of C; N2 of G) in the minor groove (Fig. 5B). In both crystal forms, lateral contacts between duplexes are mediated by bulged adenosines. All unpaired bases in the two structures are looped out and engaged in a variety of interactions that comprise the backbones, base pairs, and bulged As from adjacent duplexes as well as coordinated water molecules.

Lattice interactions of bulged adenosines

The extrahelical conformations of bulged As create diverse interactions between duplexes in the SPM and SPD crystal lattices. The interactions observed for some of the bulges suggest a stable arrangement with little room for conformational change. Others are less restricted by the interactions with neighboring residues as apparent from the smaller number of hydrogen bonds and van der Waals contacts as well as relatively high B factors for atoms of bulged As. The local environment for each of the bulges and the resulting interactions in

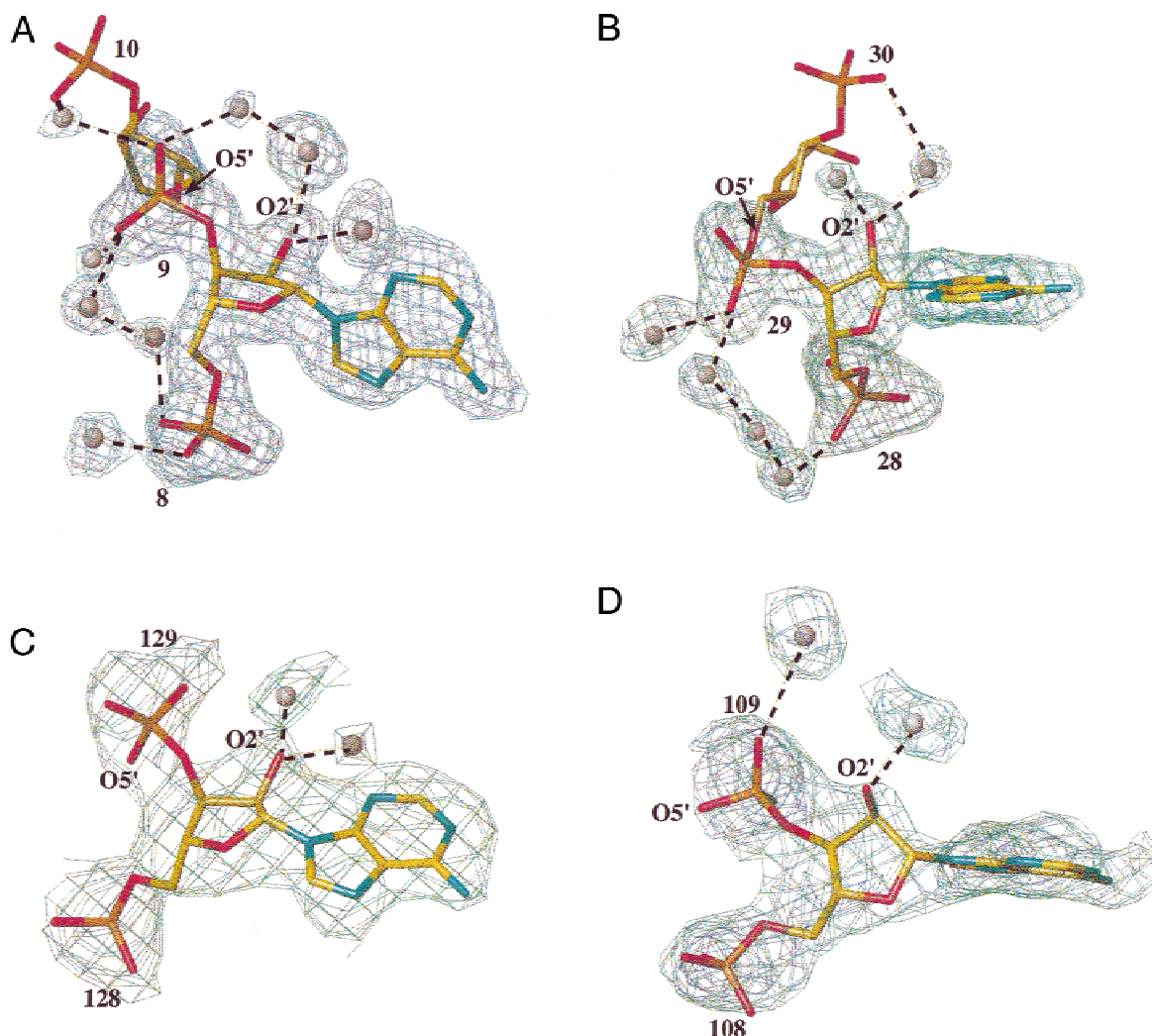


FIGURE 4. $(2F_o - F_c)$ Fourier sum electron density maps around four individual bulge regions. **A:** SPM8; **B:** SPM28; **C:** SPD128; **D:** SPD108. The maps are contoured at 1σ , water molecules are drawn as filled circles in gray, hydrogen bonds are dashed, and selected oxygen atoms are labeled. RNA atoms are colored yellow, red, blue, and orange for carbon, oxygen, nitrogen, and phosphorus, respectively.

the SPM- and SPD-form crystal lattices are depicted in Figures 6 and 7, respectively.

In the SPM-form the A8 bulge is tucked into the minor groove of an adjacent helix (Fig. 6A). Its 2'-hydroxyl group forms water-mediated hydrogen bonds to 2'-hydroxyls of riboses in both backbones of the neighboring duplex as well as to the exocyclic O2 atoms of cytosines from opposite strands. The adenine moiety of the bulged residue stacks onto the ribose of C122, resulting in a close contact between ribose O4' and the six-membered ring of the base. This type of stacking between nucleoside sugar and base from adjacent residues, either intra- or intermolecular, occurs quite frequently and was previously analyzed in the context of left-handed Z-DNA (Egli & Gessner, 1995). In addition to this interaction, the arrangement of the adenine base in the minor groove is stabilized by two hydrogen bonds between its N1 and N3 atoms and 2'-OH and N2, re-

spectively, of the 5'-terminal G121 residue from the neighboring duplex. In the SPD form, A8 has slightly shifted its position away from the minor groove toward the backbone (Fig. 7A). The phosphate group of residue C122 from the adjacent duplex now stacks onto the base moiety of A8 and the 2'-OH of the latter is hydrogen bonded to a phosphate oxygen. A spermidine molecule is located nearby but does not directly participate in the backbone–bulge interaction.

Similar environments in the two crystal forms are also observed for the A28 and A128 bulges (Figs. 6B and 7B, respectively). In both lattices, the base moiety of one of the bulged residues is sandwiched between the base of the other and the ribose of a third duplex. However, in the SPM-form lattice, the adenine of residue 128 is sandwiched whereas in the SPD form, this role is adopted by the adenine of residue 28. Moreover, the stacking in the former involves the six-membered

TABLE 1. Selected crystal data, data collection, and refinement parameters.

Structure	SPM form	SPD form
Crystallization		
DNA	0.72 mM	0.72 mM
Buffer	20 mM Na-cacod., pH 6.9	20 mM Na-cacod., pH 6.9
Polyamine	spermine, 25 mM	spermidine, 25 mM
MPD	40%	40%
Crystal data		
Space group	$P2_12_12_1$	$P2_12_12_1$
<i>a</i> (Å)	30.53	27.69
<i>b</i> (Å)	45.22	47.71
<i>c</i> (Å)	162.02	113.62
Asymmetric unit	3 duplexes/1 spermine	2 duplexes/1 spermidine
<i>V</i> (Å ³)/bp	1,695	1,705
Data collection		
X-ray source/detector	APS/MARCCD	rotating anode/R-AXIS-IIc
Temperature	120 K	120 K
Resolution (Å)	1.65	2.4
Crystal mosaicity	0.7	1.5
No. of unique reflections	26,875	6,180
Completeness (%)	97.4	94.6
R_{merge}^a	0.042	0.079
Refinement statistics		
No. of DNA/polyamine atoms	1,380/14	920/10
No. of waters	335,217 (occup. 1) + 118 (part. occup.)	81 (occup. 1)
Rms distances (Å)/angles (°)	0.011/1.54	0.013/2.03
Resolution (last shell) (Å)	10–1.65 (1.71–1.65)	10–2.40 (2.49–2.40)
Sigma cutoff	1	2
No. of reflections (last shell)	24,925 (1,169)	5,951 (594)
R_{work}^b (last shell)	21.7 (28.5)	24.9 (33.2)
R_{free}^c (last shell)	24.5 (28.1)	27.7 (35.8)

$$^a R_{\text{merge}} = \frac{\sum_{hkl} \sum_i |I(hkl)_i - \langle I(hkl) \rangle|}{\sum_{hkl} \sum_i \langle I(hkl)_i \rangle}$$

$$^b R\text{-factor} = \frac{\sum_{hkl} |F(hkl)_o - F(hkl)_c|}{\sum_{hkl} F(hkl)_o}$$

^cFor 10% of the data (Brünger, 1992).

rings of adenines whereas in the latter, the positions of bases relative to one another have shifted and stacking now occurs between the five-membered ring of A128 and the six-membered ring of A28. In both lattices, the sandwiched base forms direct hydrogen bonds to the N2 and 2'-OH atoms of G1 from the neighboring duplex that also contributes the ribose of C2 to the base-base-sugar stack. In the SPM-form lattice, the 2'-hydroxyl group of the sandwiched A128 is located in the center of the minor groove of the adjacent duplex (Fig. 6B). Thus, it forms water-mediated hydrogen bonds to N2 of G1 as well as to O2 and 2'-OH of U31.

In the SPM-form crystal lattice, the remaining bulges A108, A208, and A228 get to lie close together (Fig. 6C). In contrast to the above interactions involving base-base or base-sugar stacking and intricate hydrogen bonding networks between bulged residues and the backbones and minor grooves of adjacent duplexes, the environments observed with these three bulges appear conformationally less restrictive. A108 and A208 are hydrogen bonded via their N1 and N6 atoms, respectively, and the relative orientation of base and sugar is fixed by an intranucleoside hydrogen bond between

N3 and 2'-OH in both cases. The base plane of A228 is oriented roughly perpendicular to the base plane of A108, with N7 and C8 of the former pointing into the base plane of the adjacent adenine. Similarly, the only contact to a neighboring duplex that is observed for the A108 bulge in the SPD-form crystal lattice is a hydrogen bond between its N6 atom and a nonbridging phosphate oxygen of residue G110 (Fig. 7C).

Local and global packing effect on the duplex geometry

All 10 crystallographically independent TpC/GpA base-pair steps containing the bulged adenines along with the corresponding steps in two earlier crystal structures (Portmann et al., 1996) are depicted in Figure 8 and local helical parameters are listed in Table 2. For each step in the RNA/DNA duplex, individual and average helical parameters based on all structures were calculated (Table 2). In most cases (except for bulges SPM8 and SPM128) the TpC/GpA step has a low twist ($\sim 20^\circ$) and a negative shift (approximately -0.7 Å).

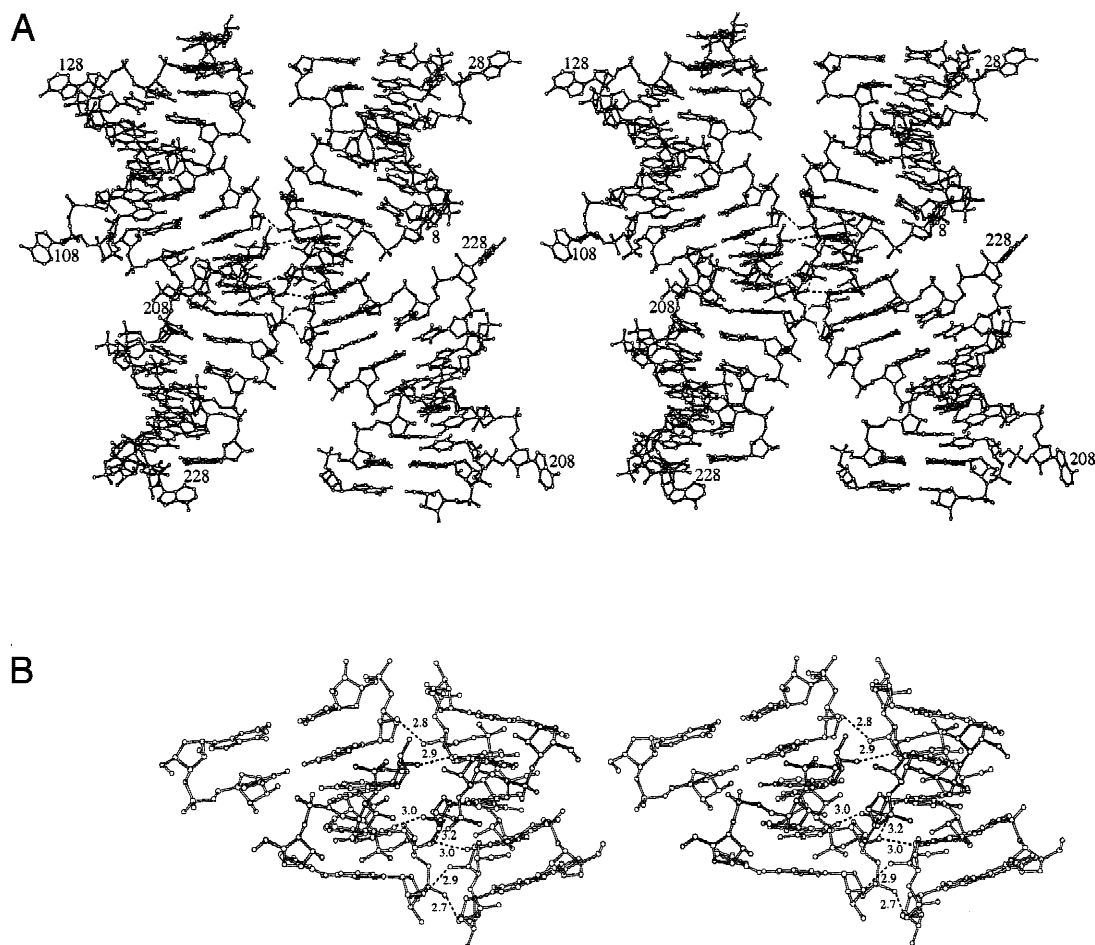


FIGURE 5. The 2'-hydroxyl zipper mediating lateral contacts between duplexes in the SPM-form crystal lattice. **A:** Stereo diagram of the overall view of the lattice contacts between four duplexes. Interactions involving 2' oxygens are drawn as thin dashed lines. **B:** Close-up of the 2'-hydroxyl zipper featuring hydrogen bonds between 2'-OH groups, between 2'-OH and phosphate oxygens, as well as between 2'-OH and base functions. Hydrogen bonds are dashed and distances are in angstroms.

Values for the roll angle range from negative (approximately -6°) to positive ($\sim 11^\circ$). In the U46 structure, the twist value is close to that found in standard A-DNA. The TpC/GpA steps comprising the SPM8 and SPM128 bulges are characterized by large twists ($\sim 50^\circ$), and positive shifts ($\sim 2 \text{ \AA}$) and rolls ($\sim 9^\circ$). In all cases, the slide is more negative than that found at central steps in the RNA/DNA duplex. In some cases (bulges SPM8, SPM128, and SPM208) significant positive rolls are found at TpC/GpA steps. However, as shown in Table 2, the largest rolls in the RNA/DNA duplex are observed at CpG steps adjacent to the TpC/GpA steps bracketing bulged As. A superposition of the three RNA/DNA duplexes constituting the asymmetric unit in the SPM-form crystals is shown in Figure 9.

The change from *adjacent* to *in-line*: Correlations among geometric parameters

The 10 bulge regions in the two crystal forms have different crystallographic environments and, conse-

quently, display a range of geometries in terms of the *adjacent* and *in-line* arrangements discussed earlier. Thus, the crystal packing forces, by acting differently on the individual bulge regions, happen to "freeze" them in different points along a potential reaction pathway. In addition, the conformations of certain bulges are affected by intranucleotide hydrogen bonds between 2'-OH and base or phosphate (see Fig. 6C). Selected geometric parameters for the bulged residues and the 3'-adjacent regions are listed in Table 3. An overview of the conformations trapped in this manner is shown in Figure 8, representing *adjacent* and near *in-line* arrangements. For comparison we have also included two previously studied DNA bulges in this analysis (termed U45 and U46, the 2'-hydroxyl groups were modeled onto the deoxyriboses; Portmann et al., 1996). Most of the bulges display an *adjacent* orientation with O2'(A)-P(C)-O5'(C) angles of around 90° . However, in three cases (including U46), the conformations of the bulged A and the 3'-adjacent residue generate a near *in-line* geometry with the above angle opened up

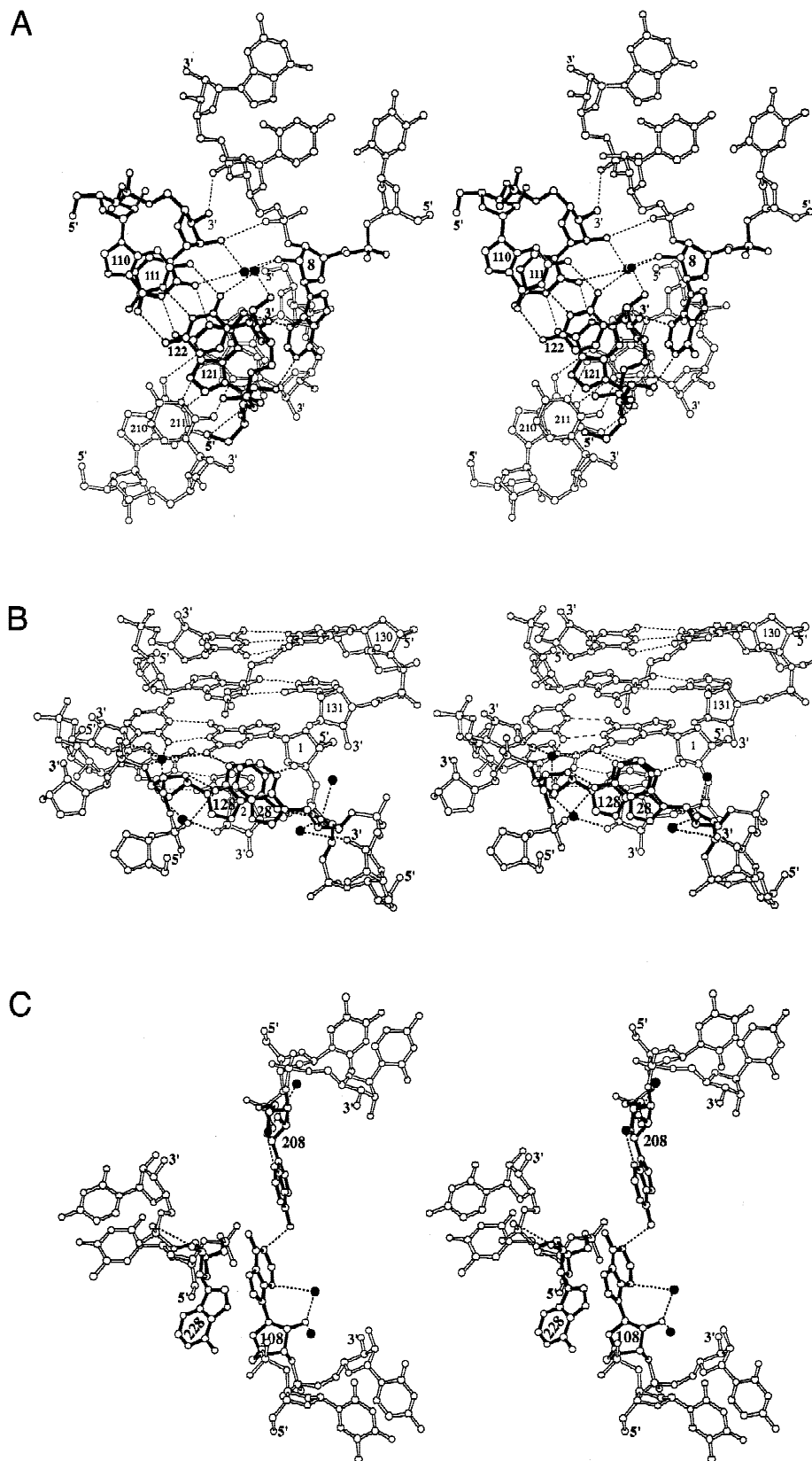


FIGURE 6. Three stereo diagrams depicting the interactions of bulged As in the SPM-form crystal. **A:** A8 (solid bonds) stacking on the ribose of residue rC121 in the minor groove formed by two adjacent duplexes (drawn with solid (top duplex) and open (bottom duplex) bonds, respectively). **B:** Stacking of A28 and A128 (solid bonds), with the latter being stacked on the ribose of residue rC2 from a third duplex. **C:** Interactions between A108, A208, and A228 (all drawn with solid bonds) from three different duplexes. Hydrogen bonds are drawn as dashed lines, water molecules are drawn as filled circles, the polarities of strands are indicated, and selected residues are labeled.

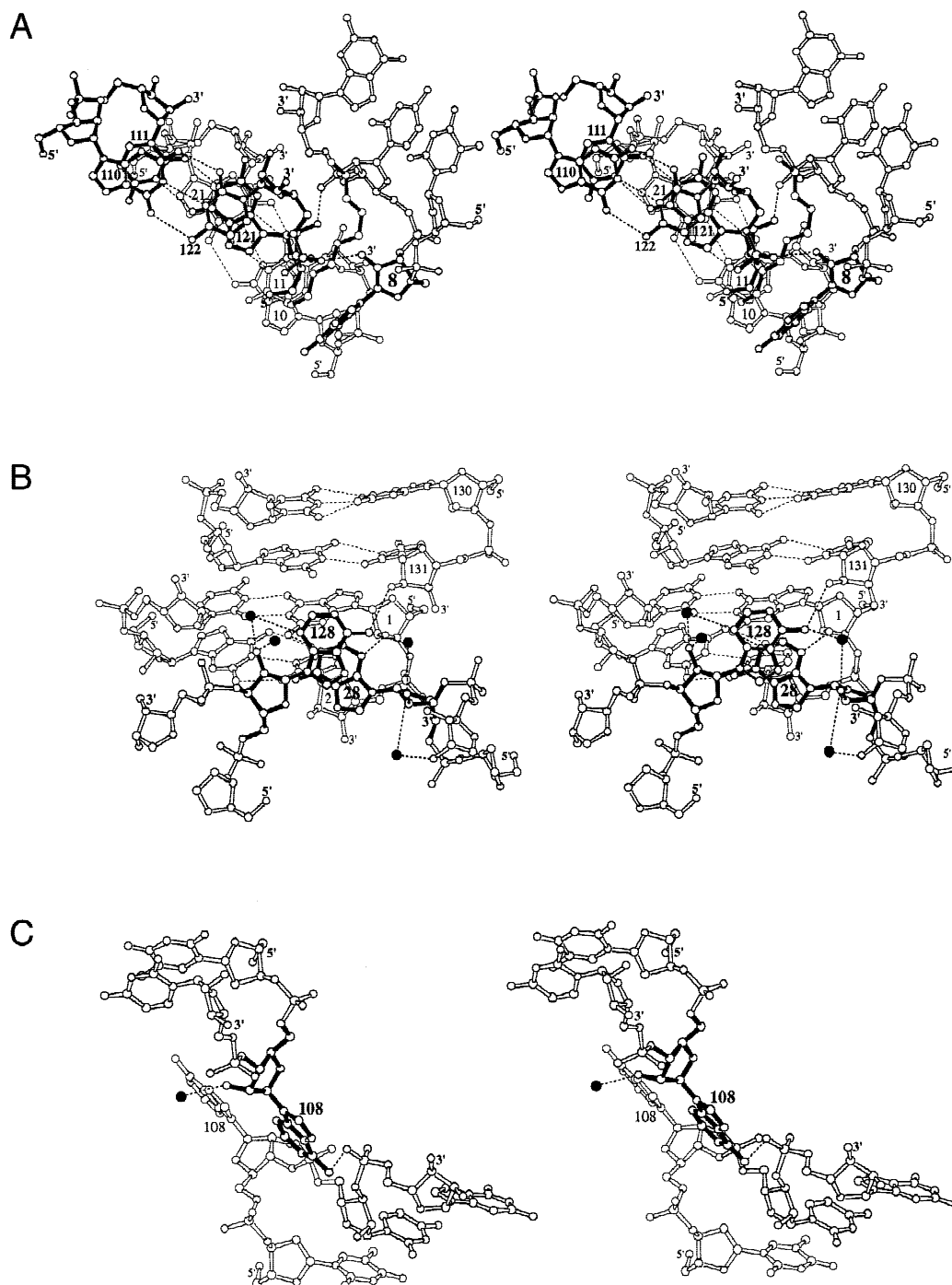


FIGURE 7. Three stereo diagrams depicting the interactions of bulged As in the SPD-form crystal. **A:** Close contact between A8 (solid bonds) and the backbone of a second duplex (base pairs drawn with solid bonds; the stacked base pairs of a third duplex are drawn with open bonds). **B:** Stacking of A28 and A128 (solid bonds), with the former being stacked on the ribose of residue rC2 from a third duplex. **C:** A108 interacting with a phosphate group from an adjacent duplex. Hydrogen bonds are drawn as dashed lines, water molecules are drawn as filled circles, the polarities of strands are indicated, and selected residues are labeled. In **A**, the spermidine molecule is drawn with solid bonds and the radius of nitrogen atoms is smaller than that of carbon atoms.

(Table 3). The transition from *adjacent* to more *in-line* appears to be accompanied by a change in the sugar pucker of the bulged residue and a shortening of the distance between the 2'-OH of the bulge and the 3'-adjacent phosphorus atom. Further hallmarks of this

transition are extended distances between the 2' oxygens of bulged adenines and 3'-adjacent Cs for near *in-line* states (data not shown).

To identify covariation between the 14 included geometric parameters, linear correlation coefficients were

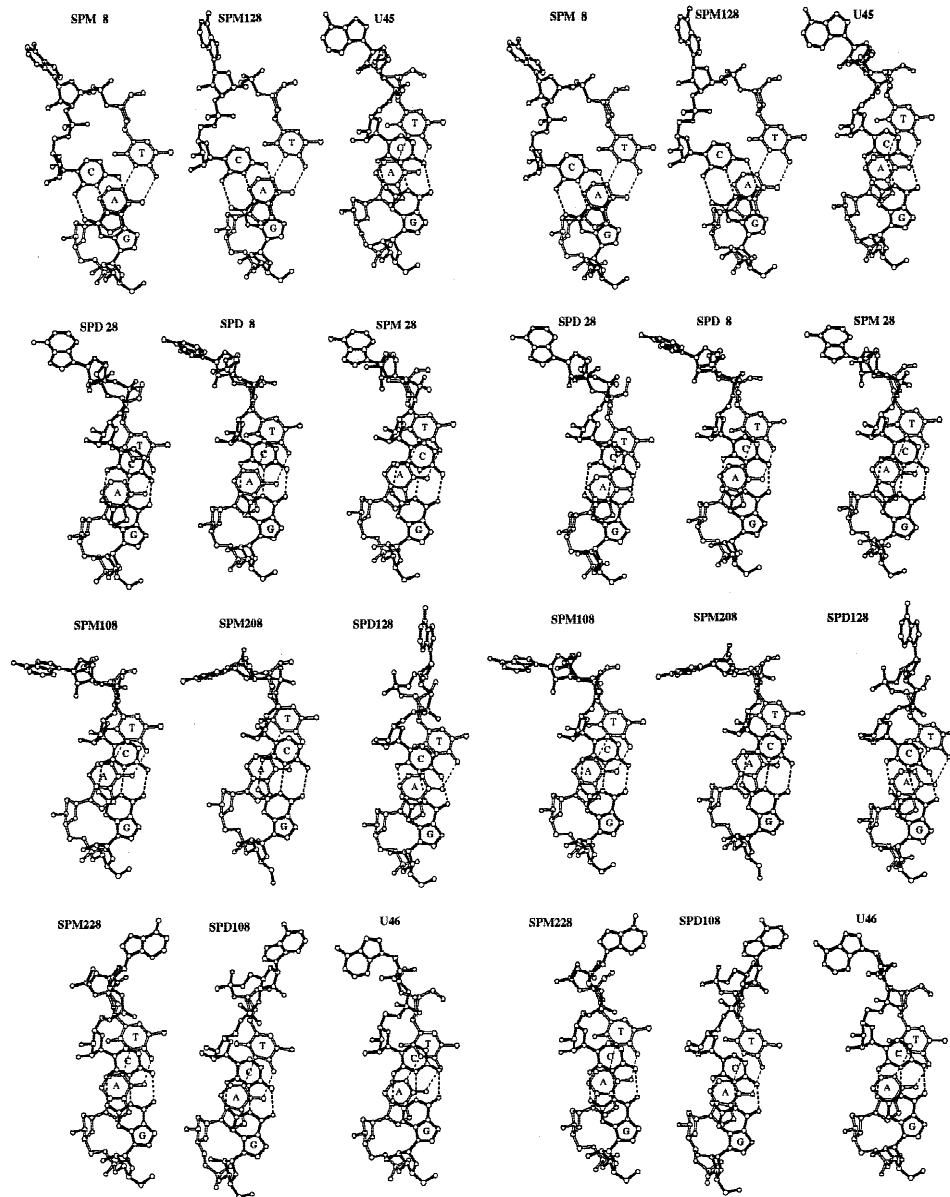


FIGURE 8. Stereo diagram depicting 12 individual crystallographically observed conformations of the A-bulge and the flanking T-A (bottom, open bonds) and C-G (top, solid bonds) base pairs. The order of the observations (proceed from left to right and then top to bottom) is the same as in Table 3 and demonstrates the gradual change from an *adjacent* arrangement between O2' (bulge) and scissile P-O5' bond (3'-adjacent C) to a near *in-line* one. Top row (left to right): SPM8, SPM128, U45 (NDB code UHK045; Portmann et al., 1996); second row: SPD28, SPD8, SPM28; third row: SPM108, SPM208, SPD128; bottom row: SPM228, SPD108, U46 (NDB code UHK046; Portmann et al., 1996).

calculated for all possible pairs among them and the resulting correlation matrix is shown in Table 4. In our analysis, we focused on correlations between parameters with a significance level of 0.01. Obviously there are many other pairs that are more weakly correlated (Table 4). However, a significance cutoff of 0.01 was chosen to simplify the task and to obtain a clearer picture of the codependencies among the distances and torsion angles that were thought to be relevant for describing the conformational change from *adjacent* to *in-line*. Among correlated pairs with suitable signifi-

cance several can be considered trivial; in other words one parameter is a function of the other. Thus, the pseudorotation phase angle P is a function of the δ torsion angle. Therefore, in cases of correlations that involve P and δ , only P was considered. Similarly, torsion angle β in T7 appears to be strongly correlated with the same angle in the bulged residue (Table 4). Closer inspection of the conformation of both β angles in all 12 cases (Table 3) shows that this angle varies only slightly and falls into the *ap* range for all residues. This is in fact what is observed in the standard double

TABLE 2. Selected local inter-base-pair parameters.^a

Step ^b	Shift (Å)	Slide (Å)	Rise (Å)	Tilt (°)	Roll (°)	Twist (°)
1 G1–C2	–0.1(3)	–1.8(2)	3.2(2)	0(4)	5(3)	41(4)
2 C2–G3	0.3(3)	–2.4(2)	3.8(2)	2(2)	13(5)	36(5)
3 G3–A4 bulge	0(1)	–1.8(5)	3.3(1)	–1(2)	3(5)	27(11)
SPM8	2.00	–1.45	3.57	1.83	10.81	49.03
SPM128	2.11	–1.38	3.38	0.01	8.50	50.12
U45	–0.80	–2.03	3.49	–3.58	2.54	19.72
SPD28	–0.73	–1.39	3.22	0.37	0.00	21.90
SPD8	–0.70	–1.53	3.15	–5.13	7.66	19.77
SPM28	–1.38	–2.36	3.28	–1.46	1.43	21.03
SPM108	–0.78	–2.09	3.34	–2.30	7.85	21.35
SPM208	–1.38	–2.60	3.34	–3.56	8.67	20.89
SPD128	–0.10	–1.37	3.46	–0.44	–4.47	18.23
SPM2238	–0.77	–2.18	3.30	0.64	1.59	26.58
SPD108	–1.44	–2.09	3.19	–0.74	–6.19	24.89
U46	–0.62	–1.06	3.33	1.24	0.32	33.98
4 A4–T5	–0.3(7)	–1.1(3)	3.1(2)	2(2)	8(3)	30(3)
5 T5–A6	0.0(3)	–1.2(3)	3.5(3)	0(1)	6(4)	34(2)

^aCalculated with the program CURVES (Lavery & Sklenar, 1989).

^bAverage values for base pairs in the two duplex halves with standard deviations in parentheses.

helical families as well. A further correlation between backbone torsion angles that is observed in the bulged duplexes here and is well known from the structural analyses of B-form DNA (Dickerson et al., 1982) and DNA-intercalator complexes (Egli, 1994) is the one between ϵ and ζ (Fig. 10A). The two angles are negatively correlated and are clustered around the so-called B_I and B_{II} types.

Geometric parameters that vary in a correlated fashion when the distance between O2'(A) and P(C) gets shorter and the O2'(A)-P(C)-O5'(C) angle opens up (the move from *adjacent* to *in-line*) are γ , P , ϵ , and ζ of A (Table 4). Bulged residues whose 2' oxygens display an *adjacent* orientation relative to the P-O5' bond of the residue C9 are associated with a +*sc* conformation

of γ , a C2'-*endo* sugar pucker, and ϵ and ζ angles that lie in the -*sc* range (Table 3). Bulged residues whose 2' oxygens display a near *in-line* orientation relative to the P-O5' bond of residue C9 (SPM228, SPD108, and U46; Table 3) are associated with a -*sc* or *ap* conformation of γ , a C3'-*endo* sugar pucker, and ϵ and ζ angles that lie in the *ap* and +*sc* ranges, respectively. Concerning the relative orientation of O2' and P-O5', the SPM228 bulge features a conformation that is intermediate between *adjacent* and *in-line*: The O2'...P distance is about 0.3 Å shorter than for *adjacent* orientations and the O2'-P-O5' angle is 117°. Its chimerical character is also apparent from the C2'-*endo* pucker (*adjacent* type) and ϵ and ζ angles that are close to those observed with the above near *in-line* conformations. Correlation dia-

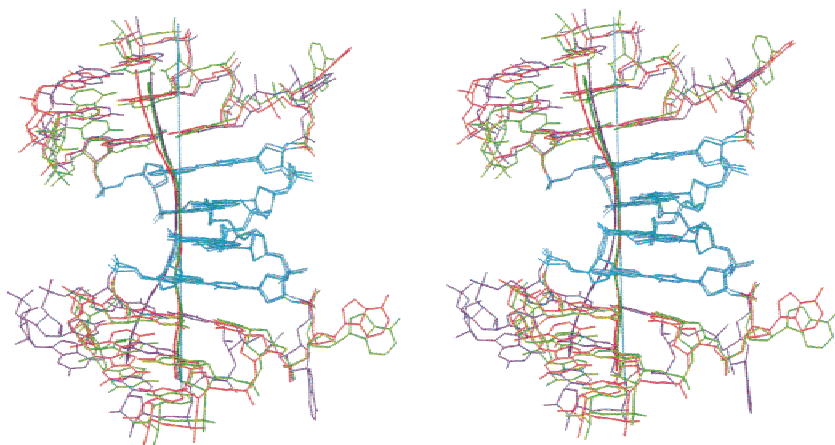


FIGURE 9. Stereo diagram of a superposition of the three duplexes constituting the asymmetric unit in the SPM-form crystal. The central d(ATAT) sections are highlighted in cyan and A bulges together with the remaining duplex portions are colored in blue, red, and green, with the helical axes (calculated with the program CURVES; Lavery & Sklenar, 1989) depicted in matching colors. The drawing illustrates the kinking of the fragments into the major groove at the interface between the central tetramer (straight helical axis colored in cyan) and the flanking RNA trimer portions.

TABLE 3. Backbone torsion angles and glycosyl torsion angles (in degrees) of individual A bulges, including 3'-adjacent ($n + 1$) backbone regions as well as distances (in angstroms) and angles between 2'-OH and phosphorus and P-O5' bond, respectively.^a

Bulge	Chi	Alpha	Beta	Gamma	Pucker	Delta	P	Epsilon	Zeta	Alpha1	Beta1 ^b	Angle ^c	Dist1 ^d	Dist2 ^e
SPM 8	-101.0	82.8	176.1	56.3	C2'-endo	145.5	166.9	-107.7	-64.7	-57.3	-150.8	71.3	4.0	4.8
SPM128	-95.7	-64.7	-149.2	52.7	C2'-endo	152.3	169.0	-97.3	-57.9	-64.7	-149.2	78.7	4.2	5.6
U45	146.5	71.4	-161.5	25.3	C2'-endo	149.9	164.6	-82.1	-56.9	-73.0	161.6	77.7	4.1	4.7
SPD 28	-81.3	91.6	-139.0	38.9	C2'-endo	134.7	152.7	-98.9	-63.3	-65.5	143.3	78.6	4.0	4.7
SPD 8	-106.0	67.7	-130.6	51.8	C2'-endo	148.0	153.2	-94.6	-77.4	-85.6	136.6	81.3	3.9	4.8
SPM 28	-74.3	92.0	-149.0	42.9	C2'-endo	138.5	149.8	-101.1	-60.6	-73.2	146.0	79.5	4.0	4.6
SPM108	-132.8	86.9	-145.6	42.9	C2'-endo	136.4	156.2	-88.7	-74.4	-64.9	124.0	83.9	4.2	4.9
SPM208	-162.6	-33.6	-162.5	-177.9	C4'-exo	97.2	61.7	-72.9	-46.2	-77.8	147.9	110.3	4.0	4.5
SPD128	163.7	117.5	177.9	-62.2	C2'-endo	141.7	160.6	-124.7	22.1	-138.8	-153.8	104.3	3.7	3.5
SPM228	-86.5	117.9	-117.0	-76.8	C2'-endo	149.1	161.0	-137.5	41.6	44.3	152.5	117.2	3.8	3.3
SPD108	-102.9	126.9	-165.2	-54.4	C3'-endo	83.9	29.6	-153.2	136.0	157.8	165.8	136.7	3.8	3.7
U46	69.0	-47.2	164.7	-170.1	C3'-endo	83.3	28.3	-154.5	89.4	-67.2	-159.4	144.1	3.8	3.5

^aCalculated with the program CURVES (Lavery & Sklenar, 1989).^bTorsion angles chi to zeta belong to the bulged rA and alpha1 and beta1 belong to the 3'-adjacent rC.^cRefers to the O2'(A)-P(C)-O5'(C) angle.^dRefers to the distance between O2'(A) and P(C).^eRefers to the distance between O2'(A) and O1P(C).**TABLE 4.** Matrix with linear correlation^a coefficients r for 14 geometric parameters^b based on 12 experimental observations.

	Chi(n)	Epsilon($n - 1$)	Zeta($n - 1$)	Alpha(n)	Beta(n)	Gamma(n)	Delta(n)	P(n)	Epsilon(n)	Zeta(n)	Alpha($n + 1$)	Beta($n + 1$)	O2'-P-O5'($n, n + 1$)	O2'...P($n, n + 1$)
Chi(n)	1.000													
Epsilon($n - 1$)	-0.265	1.000												
Zeta($n - 1$)	0.416	-0.730	1.000											
Alpha(n)	0.084	-0.378	0.241	1.000										
Beta(n)	0.486	-0.139	0.120	-0.038	1.000									
Gamma(n)	-0.154	0.365	-0.632	0.342	-0.248	1.000								
Delta(n)	0.082	0.166	-0.526	0.273	-0.093	0.737	1.000							
P(n)	0.075	0.167	-0.519	0.310	-0.061	0.752	0.988	1.000						
Epsilon(n)	-0.239	0.383	-0.367	-0.194	-0.444	0.406	0.461	0.483	1.000					
Zeta(n)	0.245	-0.552	0.601	0.110	0.260	-0.630	-0.677	-0.705	-0.907	1.000				
Alpha($n + 1$)	-0.345	-0.311	0.128	0.321	-0.330	-0.142	-0.412	-0.448	-0.558	0.653	1.000			
Beta($n + 1$)	-0.360	0.054	0.145	0.411	-0.815	0.088	-0.029	-0.042	0.296	-0.120	0.376	1.000		
O2'-P-O5'($n, n + 1$)	0.230	-0.426	0.657	-0.112	0.183	-0.846	-0.791	-0.827	-0.737	0.918	0.506	-0.023	1.000	
O2'...P($n, n + 1$)	-0.354	0.588	-0.684	-0.335	-0.484	0.553	0.370	0.398	0.743	-0.726	-0.247	0.134	-0.654	1.000

^aLinear correlation coefficients >0.708 (shaded entries) have a significance level of 0.01 (Walker & Lev, 1953).^b n , ($n + 1$) and ($n - 1$) refer to the bulged rA, the 3'-adjacent rC and the 5'-adjacent dT, respectively.

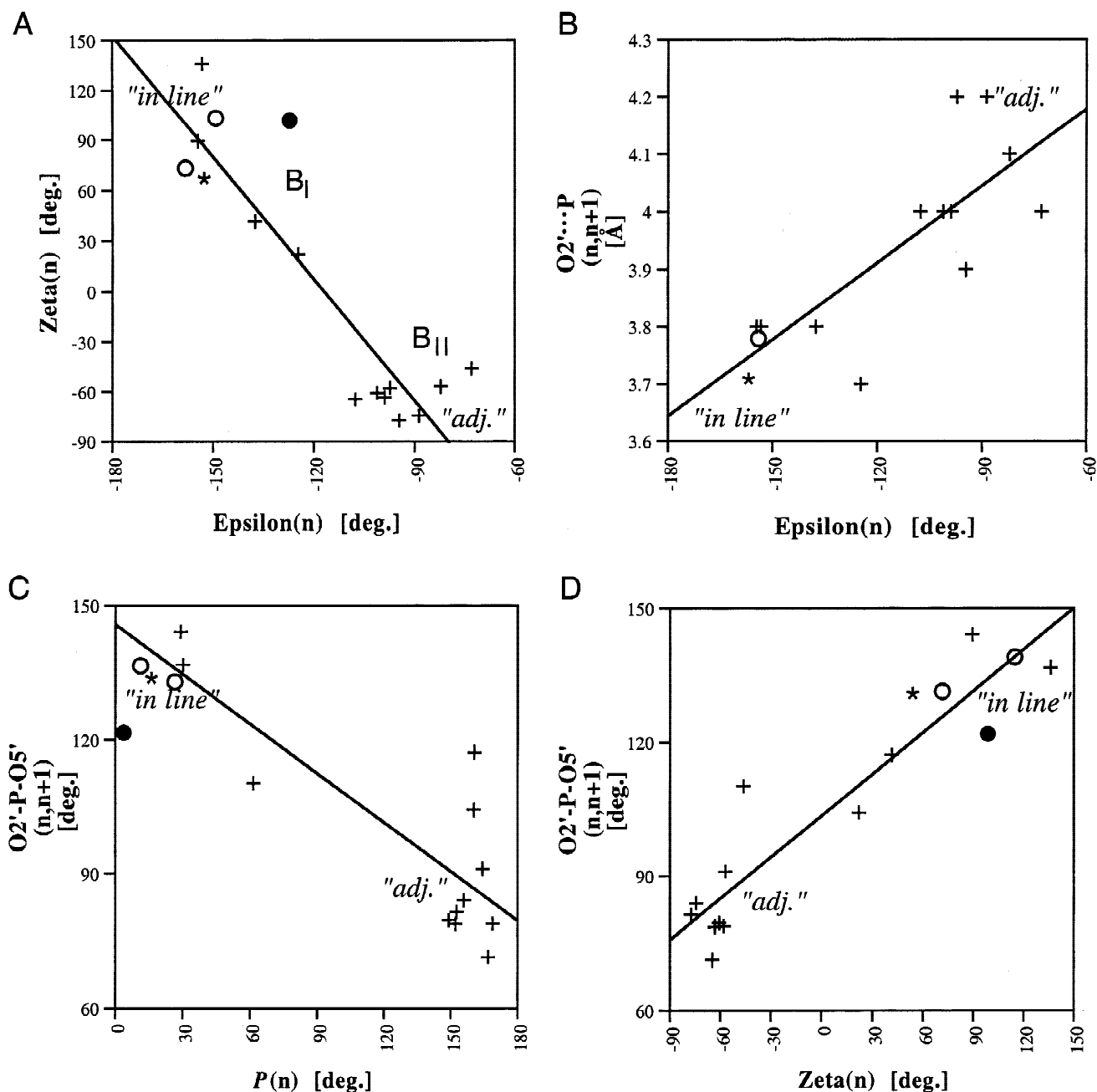


FIGURE 10. Linear correlation diagrams for selected geometrical parameters based on the analysis summarized in Table 4 (x axis: independent variable; y axis: dependent variable). **A:** Backbone torsion angles ζ versus ϵ . **B:** $O2' \cdots P$ distance versus torsion angle ϵ . **C:** $O2'-P-O5'$ angle versus pseudorotation phase angle P . **D:** $O2'-P-O5'$ angle versus torsion angle ζ . n : the bulged residue; $n+1$: a 3'-adjacent cytidine. Data points corresponding to the 12 observations in the SPM- and SPD-form crystals and the U45 and U46 structures are shown as crosses. Additional data points based on the conformations of bulged adenosines in recent crystal structures of all-RNA molecules are included for comparison and are consistent with our data. Filled circles: bulge in the RNA chain of a nonameric DNA/RNA hybrid (Sudarsanakumar et al., 2000); open circles: HIV-1 RRE high affinity Rev binding site (Ippolito & Steitz, 2000); asterisks: Rev binding element of HIV-1 (2 duplexes; Hung et al., 2000). Two data points (\bullet and \circ) missing in **B** feature values for the $O2' \cdots P$ distance that lie outside the depicted range.

grams between ϵ and $O2' \cdots P$ distance as well as between pucker and ζ and $O2'-P-O5'$ angle are depicted in Figure 10.

Put into the three dimensional-structural context, the transition from *adjacent* to *in-line* in the bulged helix

goes along with a change of pucker in the bulged residue from nonhelical to helical ($C3'-endo$). As the sugar conformation changes, the geometry of the backbone on the 5' side (γ) has to adapt and the elbow formed by the $C3'-O3'$ (torsion angle ϵ) and $O3'-P$ bonds (torsion

angle ζ) on the 3' side folds down to make way for the 2' oxygen. The reader may follow this sequence of events by looking at Figure 8 and proceeding downward, starting with the *adjacent* conformations in row 1. Perhaps not surprising, the overall conformational change does not depend on the nucleosidic angle χ (see Tables 3 and 4), and Figure 9 illustrates the conformational freedom of the adenine base. This is consistent with the results of a crystallographic study of the bulged helix II in 5S rRNA from *Xenopus laevis* (Xiong & Sundaralingam, 2000).

The requirement for a C3'-*endo* conformation of the looped-out nucleotide to bring O2' and P-O5' bond *in-line* differs from the situation in the hammerhead ribozyme, where the pucker of the nucleotide at the cleavage site supposedly has to repucker from a helical conformation to the C2'-*endo* type to allow for an *in-line* orientation (Murray et al., 1998). However, similar to the results of structural studies with hammerhead ribozymes that had all furnished molecules displaying *adjacent* (or ground state) structures, the *adjacent* orientation also appears to be preferred by the bulged duplexes studied here. One may envision an intranucleotide hydrogen bond between 2'-OH and phosphate group that could stabilize the *in-line* orientation. Indeed, such an interaction occurs in SPM228 (Fig. 6C), but in all other cases, the distance between the two moieties is too long for formation of a hydrogen bond. Therefore, it appears that an *adjacent* conformation may be energetically more stable relative to a near *in-line* one. It is very likely that metal ions (e.g., Mg²⁺) affect the energetics of this conformational equilibrium and may tilt the balance in favor of the *in-line* arrangement. Despite extensive attempts, no metal ions could be located in difference Fourier electron density maps based on data from crystals of the bulged fragment soaked in Mg²⁺ or Mn²⁺ solutions. However, it is noteworthy that a recently determined crystal structure of the dimerization initiation site of genomic HIV-1 RNA revealed coordination of a Mg²⁺ to the pro-*R*_P oxygen of the phosphate located 3' adjacent to a bulged adenosine (Ennifar et al., 1999).

CONCLUSIONS

The bulged adenosine introduces conformational flexibility at the global and the local level. The main consequence globally is the bending of the double helix to various degrees. Local conformational changes appear to be chiefly responsible for lining up the 2'-OH of the bulge and the scissile phosphate bond and therefore indirectly for cleavage. Most notable among them are the repuckering of the bulged residue and the correlated changes in its ϵ and ζ torsion angles. All bulged adenosines in the two analyzed crystal forms adopt extrahelical arrangements. As described in more detail in an earlier analysis of bulged A-type duplexes, this

may be due to the unpaired A being located between pyrimidines (Portmann et al., 1996, and cited references). In addition, close packing of duplexes in the crystal provides numerous opportunities for looped-out nucleotides to interact with adjacent duplexes or other bulges. This may be different in solution where the lack of tight interactions between duplexes may favor an intrahelical arrangement of the unpaired nucleotide. Thus, it is clear that our analysis can only shed light on the conformational changes that precede the *in-line* orientation of 2'-OH and scissile bond in extrahelical bulged nucleotides. Modeling studies suggested that an intrahelical arrangement of an unpaired nucleotide in principle permits sufficient conformational flexibility of the backbone to bring 2'-OH and scissile bond *in-line* (Hüsken et al., 1996).

MATERIALS AND METHODS

Oligonucleotide synthesis, purification, and crystallization

The 11mers for the crystallographic studies and cleavage experiments in solution were synthesized on 10 μ mol scales on a Pharmacia Expedite synthesizer, using standard phosphoramidite chemistry in combination with 2'-*O*-TBDMS protected RNA synthons (Usman et al., 1992; Wincott et al., 1995). Following deprotection, oligonucleotides were purified on a C4 RP-HPLC column (Rainin Dynamax). The buffer was 50 mM triethylammonium acetate, pH 7.0, and the eluent was acetonitrile. After lyophilization, the concentrations of aqueous stock solutions were adjusted to 5 mM.

RNA cleavage experiments

The 11mer r(GCGAUUAACGU) (60 pmol) was 5'-radioactively labeled using T4 polynucleotide kinase (Gibco). The labeled RNA was gel purified over a 19% polyacrylamide gel. The following final cleavage reaction conditions were mixed in 20 μ L samples: 30 nM to 100 nM labeled RNA, 0 to 5 mM MgCl₂, 100 mM Tris-HCl, 6 \leq pH \leq 8.0, and 100 mM sodium acetate. The probes were initially incubated at 80 °C for 1 min before cooling them to 4 °C over 30 min. All samples were then kept at 4 °C for 30 h. The reactions were precipitated, resuspended in urea loading buffer, and analyzed over 19% polyacrylamide gels and the gels interpreted on a phosphor-imager (Molecular Dynamics; Fig. 3).

X-ray crystallographic studies

Two crystal forms of the 11mer r(GCG)d(ATAT)r(AACGU) were grown by hanging drop vapor diffusion in the presence of either spermine (SPM form) or spermidine (SPD form) within a pH range of 5.5 to 9.0. Typical crystallization conditions for the two forms are listed in Table 1. Various datasets were collected on either in-house X-ray equipment or on the 5-ID beamline of the DuPont-Northwestern-Dow Collaborative Access Team (DND-CAT) at the Advanced Photon Source (APS), Argonne National Laboratory, Argonne, Illinois (Table 1).

Crystals of the spermine form diffracted to 1.65 Å resolution and contain three molecules (six bulges) per crystallographic asymmetric unit. Crystals of the spermidine form diffract to about 2.4 Å resolution and contain two molecules (four bulges) per asymmetric unit. All data were indexed and merged in the DENZO/SCALEPACK suite (Otwinowski & Minor, 1997). The structures of the two crystal forms were determined by the Molecular Replacement method (program AMoRe; Navaza, 1994), using the previously determined structure of a RNA/DNA duplex with single nucleotide bulges as a model (NDB code UHK045; Portmann et al., 1996). Refinements were carried out with the program CNS (Brünger, 1998), using the most recent parameter files (Parkinson et al., 1996). Final *R*-factors and root mean square (rms) deviations from standard geometric parameters are listed in Table 1.

Accession numbers

Structure factors and final coordinates for the SPM and SPD structures have been deposited in the Protein Data Bank and the accession codes are 1I2Y (SPM form) and 1I2X (SPD form).

ACKNOWLEDGMENTS

This work was supported by the Petroleum Research Fund, administered by the American Chemical Society (PRF AC-32434 to M.E.) and the National Institutes of Health (R01 GM-55237 to M.E.). The DuPont-Northwestern-Dow Collaborative Access Team Synchrotron Research Center at the Advanced Photon Source, Argonne, Illinois, is supported by E. I. DuPont de Nemours & Co., The Dow Chemical Company, the National Science Foundation and the State of Illinois.

Received September 22, 2000; returned for revision October 23, 2000; revised manuscript received November 28, 2000

REFERENCES

- Amiri KMA, Hagerman PJ. 1996. The global conformation of an active hammerhead RNA during the process of self-cleavage. *J Mol Biol* 261:125–134.
- Beese LS, Steitz TA. 1991. Structural basis for the 3'-5' exonuclease activity of *Escherichia coli* DNA polymerase I: A two metal ion mechanism. *EMBO J* 10:25–33.
- Brautigam CA, Steitz TA. 1998. Structural and functional insights provided by crystal structures of DNA polymerases and their substrate complexes. *Curr Opin Struct Biol* 8:54–63.
- Brown RS, Dervan JC, Klug A. 1985. Crystallographic and biochemical investigation of the lead(II)-catalyzed hydrolysis of yeast phenylalanine tRNA. *Biochemistry* 24:4785–4801.
- Brünger AT. 1992. Free R value: A novel statistical quantity for assessing the accuracy of crystal structures. *Nature* 355:472–475.
- Brünger AT. 1998. Crystallography & NMR System (CNS), Version 0.5, Yale University, New Haven, Connecticut.
- Buzayan JM, Gerlach WL, Bruening G. 1986. Non-enzymatic cleavage and ligation of RNAs complementary to a plant virus satellite RNA. *Nature* 323:349–353.
- Cate JH, Gooding AR, Podell E, Zhou K, Golden BL, Kundrot CE, Cech TR, Doudna JA. 1996. Crystal structure of a group I ribozyme domain: Principles of RNA packing. *Science* 273:1678–1685.
- Cech TR. 1987. The chemistry of self-splicing RNA and RNA enzymes. *Science* 236:1532–1539.
- Dahm SC, Derrick WB, Uhlenbeck OC. 1993. Evidence for the role of solvated metal hydroxide in the hammerhead cleavage mechanism. *Biochemistry* 32:13040–13045.
- Dahm SC, Uhlenbeck OC. 1990. Characterization of deoxy- and ribo-containing oligonucleotide substrates in the hammerhead self-cleavage reaction. *Biochimie* 72:819–823.
- Dahm SC, Uhlenbeck OC. 1991. Role of divalent metal ions in the hammerhead RNA cleavage reaction. *Biochemistry* 30:9464–9469.
- Dickerson RE, Kopka ML, Drew HR. 1982. Structural correlations in B-DNA. In: Srinivasan R, Sarma RH, eds. *Conformation in biology*. New York: Adenine Press. pp 227–257.
- Earnshaw DJ, Gait MJ. 1998. Hairpin ribozyme cleavage catalyzed by aminoglycoside antibiotics and the polyamine spermine in the absence of metal ions. *Nucleic Acids Res* 26:5551–5561.
- Egli M. 1994. Structural patterns in nucleic acids. In: Bürgi H-B, Dunitz JD, eds. *Structure correlation*, Vol. 2, New York: VCH Publishers Inc. pp 705–749.
- Egli M, Gessner RV. 1995. Stereoelectronic effects of deoxyribose O4' on DNA conformation. *Proc Natl Acad Sci USA* 92:180–184.
- Ennifar E, Yusupov M, Walter P, Marquet R, Ehresmann B, Ehresmann C, Dumas P. 1999. The crystal structure of the dimerization initiation site of genomic HIV-1 RNA reveals an extended duplex with two adenine bulges. *Structure* 7:1439–1449.
- Fedor MJ. 2000. Structure and function of the hairpin ribozyme. *J Mol Biol* 297:269–291.
- Ferré-D'Amaré AR, Zhou K, Doudna JA. 1998. Crystal structure of a hepatitis delta virus ribozyme. *Nature* 395:567–574.
- Gerlt JA. 1993. Mechanistic principles of enzyme-catalyzed cleavage of phosphodiester bonds. In: Linn SM, Lloyd RS, Roberts RJ, eds. *Nucleases*, 2nd Ed., Cold Spring Harbor, New York: Cold Spring Harbor Laboratory Press. pp 1–34.
- Grosshans CA, Cech TR. 1989. Metal ion requirements for sequence-specific endoribonuclease activity of the *Tetrahymena* ribozyme. *Biochemistry* 28:6888–6894.
- Guerrier-Takada C, Gardiner K, Marsh T, Pace N, Altman S. 1983. The RNA moiety of ribonuclease P is the catalytic subunit of the enzyme. *Cell* 35:849–857.
- Hampel A. 1998. The hairpin ribozyme: Discovery, two-dimensional model, and development for gene therapy. *Prog Nucleic Acid Res Mol Biol* 58:1–39.
- Hampel A, Cowan JA. 1997. A unique mechanism for RNA catalysis: The role of metal cofactors in hairpin ribozyme cleavage. *Chem Biol* 4:513–517.
- Hampel A, Tritz R. 1989. RNA catalytic properties of the minimum (–)sTRSV sequence. *Biochemistry* 28:4929–4933.
- Haydock K, Allen LC. 1985. Molecular mechanism of catalysis by RNA. In: Haydock K, Allen LC, eds. *Molecular basis of cancer, Part A: Macromolecular structure, carcinogens, and oncogenes*. New York: Alan R. Liss, Inc. pp 87–98.
- Herman T, Auffinger P, Scott WG, Westhof E. 1997. Evidence for a hydroxide ion bridging two magnesium ions at the active site of the hammerhead ribozyme. *Nucleic Acids Res* 25:3421–3427.
- Herman T, Auffinger P, Westhof E. 1998. Molecular dynamics investigations on the hammerhead ribozyme RNA. *Eur J Biophys* 27:153–165.
- Hough E, Hansen LK, Birknes B, Jynge K, Hansen S, Hordvik A, Little C, Dodson E, Derewenda Z. 1989. High-resolution (1.5 Å) crystal structure of phospholipase C from *Bacillus cereus*. *Nature* 338:357–360.
- Hung L-W, Holbrook EL, Holbrook SR. 2000. The crystal structure of the Rev binding element of HIV-1 reveals novel base pairing and conformational variability. *Proc Natl Acad Sci USA* 97:5107–5112.
- Hüsken D, Goodall G, Blommers MJJ, Jahnke W, Hall J, Häner R, Moser HE. 1996. Creating RNA bulges: Cleavage of RNA in RNA/DNA duplexes by metal ion catalysis. *Biochemistry* 35:16591–16600.
- Hutchins CJ, Rathjen PD, Forster AC, Symons RH. 1986. Self-cleavage of plus and minus RNA transcripts of avocado sunblotch viroid. *Nucleic Acids Res* 14:3627–3640.
- Ippolito JA, Steitz TA. 2000. The structure of the HIV-1 RRE high affinity Rev binding site at 1.6 Å resolution. *J Mol Biol* 295:711–717.
- Kim EE, Wyckoff HW. 1991. Reaction mechanism of alkaline phosphatase based on crystal structures. *J Mol Biol* 218:449–464.
- Koizumi M, Ohtsuka E. 1991. Effects of phosphorothioate and 2-amino groups in hammerhead ribozymes on cleavage rates and Mg²⁺ binding. *Biochemistry* 30:5145–5150.
- Kruger K, Grabowski PJ, Zaug AJ, Sands J, Gottschling DE, Cech

- TR. 1982. Self-splicing RNA: Autoexcision and autocyclization of the ribosomal RNA intervening sequence of *Tetrahymena*. *Cell* 31:147–157.
- Kuimelis RG, McLaughlin LW. 1996. Ribozyme-mediated cleavage of a substrate analogue containing an internucleotide-bridging 5'-phosphorothioate: Evidence for the single-metal model. *Biochemistry* 35:5308–5317.
- Lavery R, Sklenar HJ. 1989. Defining the structure of irregular nucleic acids—conventions and principles. *J Biomol Struct Dyn* 6:655–667.
- Lott WB, Pontius BW, van Hippel PH. 1998. A two-metal ion mechanism operates in the hammerhead ribozyme-mediated cleavage of an RNA substrate. *Proc Natl Acad Sci USA* 95:542–547.
- Lyne PD, Karplus M. 2000. Determination of the pK_a of the 2'-hydroxyl group of a phosphorylated ribose: Implications for the mechanism of hammerhead ribozyme catalysis. *J Am Chem Soc* 122:166–167.
- Mei H-Y, Kaaret TW, Bruice TC. 1989. A computational approach to the mechanism of self-cleavage of hammerhead RNA. *Proc Natl Acad Sci USA* 86:9727–9731.
- McKay DB. 1996. Structure and function of the hammerhead ribozyme: An unfinished story. *RNA* 2:395–403.
- Murray JB, Terwey DP, Maloney L, Karpeisky A, Beigelman L, Scott WG. 1998. The structural basis of hammerhead ribozyme self-cleavage. *Cell* 92:665–673.
- Nakano S-I, Chadalavada DM, Bevilacqua PC. 2000. General acid-base catalysis in the mechanism of a hepatitis delta virus ribozyme. *Science* 287:1493–1497.
- Navaza J. 1994. AMoRe: An automated package for molecular replacement. *Acta Cryst A* 50:157–163.
- Nesbitt S, Hegg LA, Fedor MJ. 1997. An unusual pH-independent and metal-ion-independent mechanism for hairpin ribozyme catalysis. *Chem Biol* 4:619–630.
- Nowakowski J, Shim PJ, Prasad GS, Stout CD, Joyce GF. 1999. Crystal structure of an 82-nucleotide RNA–DNA complex formed by the 10-23 DNA enzyme. *Nat Struct Biol* 6:151–156.
- Otwiński Z, Minor W. 1997. Processing of X-ray diffraction data collected in oscillation mode. *Methods Enzymol* 276:307–326.
- Parkinson G, Vojtechovsky J, Clowney L, Brünger AT, Berman HM. 1996. New parameters for the refinement of nucleic acid containing structures. *Acta Cryst D* 52:57–64.
- Perreault J-P, Wu T, Cousineau B, Ogilvie KK, Cedergren R. 1990. Mixed deoxyribo- and ribo-oligonucleotides with catalytic activity. *Nature* 344:565–567.
- Perrotta AT, Shih I-H, Been MD. 1999. Imidazole rescue of a cytosine mutation in a self-cleaving ribozyme. *Science* 286:123–126.
- Pley HW, Flaherty KM, McKay DB. 1994. Three-dimensional structure of a hammerhead ribozyme. *Nature* 372:68–74.
- Portmann S, Grimm S, Workman C, Usman N, Egli M. 1996. Crystal structures of an A-form duplex with single-adenosine bulges and a conformational basis for site-specific RNA self-cleavage. *Chem & Biol* 3:173–184.
- Prody GA, Bakos JT, Buzayan JM, Schneider IR, Bruening G. 1986. Analytic processing of dimeric plant virus satellite RNA. *Science* 231:1577–1580.
- Santoro SW, Joyce GF. 1997. A general purpose RNA-cleaving DNA enzyme. *Proc Natl Acad Sci USA* 94:4262–4266.
- Sawata S, Komiyama M, Taira K. 1995. Kinetic evidence based on solvent isotope effects for the nonexistence of a proton-transfer process in reactions catalyzed by a hammerhead ribozyme: Implication to a double-metal-ion mechanism of catalysis. *J Am Chem Soc* 117:2357–2358.
- Setlik RF, Shibata M, Sarma RH, Sarma MH, Kazim AL, Ornstein RL, Tomasi TB, Rein R. 1995. Modeling of a possible conformational change associated with the catalytic mechanism in the hammerhead ribozyme. *J Biomol Struct Dyn* 13:515–521.
- Scott WG, Finch JT, Klug A. 1995. The crystal structure of an all-RNA hammerhead ribozyme: A proposed mechanism for RNA catalytic cleavage. *Cell* 81:991–1002.
- Scott WG, Murray JB, Arnold JRP, Stoddard BL, Klug A. 1996. Capturing the structure of a catalytic RNA intermediate: The hammerhead ribozyme. *Science* 274:2065–2069.
- Sharmeen L, Kuo MYP, Diner-Gottlieb G, Taylor J. 1988. Antigenomic RNA of human hepatitis delta virus can undergo self-cleavage. *J Virol* 62:2674–2679.
- Slim G, Gait MJ. 1991. Configurationally defined phosphorothioate-containing oligonucleotides in the study of the mechanism of cleavage of hammerhead ribozymes. *Nucleic Acids Res* 19:1183–1188.
- Steitz JA, Steitz JA. 1993. A general two-metal-ion mechanism for catalytic RNA. *Proc Natl Acad Sci USA* 90:6498–6502.
- Soukup GA, Breaker RR. 1999. Relationship between internucleotide linkage geometry and the stability of RNA. *RNA* 5:1308–1325.
- Sudarsanakumar C, Xiong Y, Sundaralingam M. 2000. Crystal structure of an adenine bulge in the RNA chain of a DNA•RNA hybrid, d(CTCCTCTTC)r(gaagagagag). *J Mol Biol* 299:103–112.
- Tesmer JGG, Sunahara RK, Johnson RA, Gosselin G, Gilman AG, Sprang SR. 1999. Two-metal-ion catalysis in adenylyl cyclase. *Science* 285:756–760.
- Torres RA, Bruice TC. 2000. The mechanism of phosphodiester hydrolysis: Near in-line attack conformations in the hammerhead ribozyme. *J Am Chem Soc* 122:781–791.
- Uchimaru T, Uebayasi M, Hirose T, Tsuzuki S, Yliniemelä A, Tanabe K, Taira K. 1996. Electrostatic interactions that determine the rate of pseudorotation processes in oxyphosphorane intermediates: Implications with respect to the roles of metal ions in the enzymatic cleavage of RNA. *J Org Chem* 61:1599–1608.
- Uebayasi M, Uchimaru T, Koguma T, Sawata S, Shimayama T, Taira K. 1994. Theoretical and experimental considerations on the hammerhead ribozyme reactions: Divalent magnesium ion mediated cleavage of phosphorus-oxygen bonds. *J Org Chem* 59:7414–7420.
- Uhlenbeck OC. 1987. A small catalytic oligoribonucleotide. *Nature* 328:596–600.
- Usher DA, McHale AH. 1976. Hydrolytic stability of helical RNA: A selective advantage for the natural 3',5'-bond. *Proc Natl Acad Sci USA* 73:1149–1153.
- Usman N, Egli M, Rich A. 1992. Large scale chemical synthesis, purification and crystallization of RNA–DNA chimeras. *Nucleic Acids Res* 20:6695–6699.
- Van Tol H, Buzayan JM, Feldstein PA, Eckstein F, Bruening G. 1990. Autolytic processing reactions of a satellite RNA proceed with inversion of configuration. *Nucleic Acids Res* 18:1971–1975.
- Verma S, Vaish NK, Eckstein F. 1997. Structure-function studies of the hammerhead ribozyme. *Curr Opin Chem Biol* 1:532–536.
- Walker HM, Lev J. 1953. *Statistical inference*, New York: Holt. p 470.
- Walter NG, Burke JM. 1998. The hairpin ribozyme: Structure, assembly and catalysis. *Curr Opin Chem Biol* 2:24–30.
- Wedekind JE, McKay DB. 1999. Crystal structure of a lead-dependent ribozyme revealing metal binding sites relevant to catalysis. *Nat Struct Biol* 6:261–268.
- Westheimer FH. 1968. Pseudo-rotation in the hydrolysis of phosphate esters. *Acc Chem Res* 1:70–78.
- Westhof E. 1999. Chemical diversity in RNA cleavage. *Science* 286:61–62.
- Wincott FE, DiRenzo A, Shaffer C, Grimm S, Tracz D, Workman C, Sweedler D, Gonzalez C, Scaringe S, Usman N. 1995. Synthesis, deprotection, analysis and purification of RNA and ribozymes. *Nucleic Acids Res* 23:2677–2684.
- Wu H-N, Lin Y, Lin F, Makino S, Chang M, Lai MMC. 1989. Human hepatitis δ virus RNA subfragments contain an autocleavage activity. *Proc Natl Acad Sci USA* 86:1831–1835.
- Xiong Y, Sundaralingam M. 2000. Two crystal forms of helix II of *Xenopus laevis* 5S rRNA with a cytosine bulge. *RNA* 6:1316–1324.
- Young KJ, Gill F, Grasby JA. 1997. Metal ions play a passive role in the hairpin ribozyme catalyzed reaction. *Nucleic Acids Res* 25:3760–3766.